membranes

MDPI

Article

Analysis of Polyvinylidene Fluoride Membranes Fabricated for Membrane Distillation

Minchul Ahn [1], Hyeongrak Cho [1], Yongjun Choi [1], Seockheon Lee [2] and Sangho Lee [1,*]

[1] School of Civil and Environmental Engineering, Kookmin University, Seoul 02707, Korea; 92vet@naver.com (M.A.); rhino@kookmin.ac.kr (H.C.); choiyj1041@gmail.com (Y.C.)
[2] Water and Resource Recycle Center, Korea Institute of Science and Technology, Seoul 02792, Korea; seocklee@kist.re.kr
* Correspondence: sanghlee@kookmin.ac.kr; Tel.: +82-2-910-4529

Abstract: The optimization of the properties for MD membranes is challenging due to the trade-off between water productivity and wetting tendency. Herein, this study presents a novel methodology to examine the properties of MD membranes. Seven polyvinylidene fluoride (PVDF) membranes were synthesized under different conditions by the phase inversion method and characterized to measure flux, rejection, contact angle (CA), liquid entry pressure (LEP), and pore sizes. Then, water vapor permeability (B_w), salt leakage ratio (L_w), and fiber radius (R_f) were calculated for the in-depth analysis. Results showed that the water vapor permeability and salt leakage ratio of the prepared membranes ranged from 7.76×10^{-8} s/m to 20.19×10^{-8} s/m and from 0.0020 to 0.0151, respectively. The R_f calculated using the Purcell model was in the range from 0.598 μm to 1.690 μm. Since the R_f was relatively small, the prepared membranes can have high LEP (more than 1.13 bar) even at low CA (less than 90.8°). The trade-off relations between the water vapor permeability and the other properties could be confirmed from the results of the prepared membranes. Based on these results, the properties of an efficient MD membrane were suggested as a guideline for the membrane development.

Keywords: membrane distillation; membrane fabrication; analysis; flux; wetting; liquid entry pressure; contact angle

Citation: Ahn, M.; Cho, H.; Choi, Y.; Lee, S.; Lee, S. Analysis of Polyvinylidene Fluoride Membranes Fabricated for Membrane Distillation. *Membranes* **2021**, *11*, 437. https://doi.org/10.3390/membranes11060437

Academic Editor: Isabel C. Escobar

Received: 18 May 2021
Accepted: 5 June 2021
Published: 10 June 2021

1. Introduction

The growth of world population and industry has posed challenges associated with the imbalance between water demands and availability. The situation has been worsened by the impact of climate change, which results in unexpected fluctuations in rainfall patterns and the availability of water resources [1,2]. One of the technologies that alleviate this problem is desalination of seawater, brackish water, or wastewater [3,4]. Since desalination technique does not rely on freshwater resources, it can provide ongoing water supply by utilizing alternative water sources [5]. This is the key driver that makes the widespread adoption of desalination technology over the past decades [6–8].

However, the implementation of desalination requires a viable option for the management of brines, which is the remaining stream after the production of fresh water from seawater or impaired water sources [9,10]. Conventional desalination processes including multistage flash (MSF), multi-effect distillation (MED), and reverse osmosis (RO) result in a substantial amount of brines ranging from 40% to 60% of the feed water [11]. Since the brine exhibits a higher salinity than the feed water, its direct discharge may lead to harmful effects on marine environment and aquatic ecosystems [12]. Accordingly, it is crucial to explore novel techniques to reduce the adverse impact by reducing the volume or salinity of the brine [12].

A promising option for brine management is to develop and apply membrane distillation (MD) process that allows the reduction of the brine volume and the additional

production of fresh water [13–15]. MD is a special evaporation technique and requires hydrophobic microporous membranes to separate feed water and vapors [16–18]. Since MD is thermally driven, its operation is not limited by the osmotic pressure, allowing the treatment of high salinity brine from RO or MSF/MED processes [19,20]. Moreover, MD may use moderate-temperature thermal sources (50–70 °C) that are cheaper than high-temperature heat sources used by MSF/MED [21]. MD can be considered as a part of zero liquid discharge (ZLD) systems [22]. Many MD systems for brine management have been reported in the literature due to their potential [17,23,24]. Nevertheless, most works were done in laboratory scales [8,25].

One of the biggest hurdles MD technology faces is the availability of efficient MD membranes [26,27]. There are several commercial hydrophobic membranes for MD experiments but they are not specifically optimized for MD [23]. This is because the requirements for MD membranes are quite unique [26]. Pore wetting is a critical issue in MD processes, which affects the quality of product water. To minimize it, it is necessary to fabricate hydrophobic MD membranes or increase the liquid entry pressure (LEP) [24,28]. On the other hand, fouling and scale formation are also serious problems that reduce the flux and lifespan of MD membranes. The pretreatment of feed water as well as physical/chemical cleaning may be applied to mitigate the adverse impact of fouling and scaling [29]. Nevertheless, it is also important to improve the fouling resistance of MD membranes by surface modifications [29]. To prevent adsorptive fouling caused by hydrophobic organic matters, MD membranes should be rather hydrophilic. The pore size of the MD membranes should be as small as possible to decrease the possibility of pore wetting. On the contrary, the flux and water productivity of the MD membrane increase with an increase in the pore size [15,16]. Although numerous works have been done on the synthesis of MD membranes [28,30–36], it is still challenging to optimize its conditions due to the complex trade-offs.

Accordingly, it is necessary to implement systematic approaches to meet different requirements of MD membranes. However, only limited information is available for in-depth analysis of MD membrane characteristics. In addition to flux and rejection, more fundamental performance indexes should be used to provide insight into the multi-objective optimization of synthesis conditions for MD membranes. Herein, a novel methodology to examine the properties of MD membranes was developed and applied to several polyvinylidene fluoride (PVDF) membranes synthesized under different conditions by the phase inversion method. In previous works, protic or aprotic solvents such as methanol, propanol, butanol, octanol, and N-methyl-prrolidone were added to the non-solvent, leading to an increase in the hydrophobicity of the membrane surface [37–39]. However, these solvents are toxic, and pose threats to the environment and human health. Therefore, water and ethanol were used in this study because they are more environmentally friendly. The prepared membranes were characterized to determine flux, rejection, contact angle (CA), liquid entry pressure (LEP), and pore sizes. Then, a set of new performance measures such as water vapor permeability (B_w), salt leakage ratio (L_w), and fiber radius (R_f) were proposed. The correlations between different membrane properties were also investigated to understand the trade-offs in MD membranes. Based on this analysis, the properties of efficient MD membranes were explored.

2. Materials and Methods

2.1. Materials

PVDF was purchased from Sigma-Aldrich Co. (St. Louis, MO, USA) and its molecule weight was 530,000 g/mol. N,N-Dimethylformamide (DMF, 99.9%), lithium chloride (LiCl, 98.2%), and ethyl alcohol (EtOH, 99.9%) were supplied by Samchun Inc. (Gyeonggi-do, Korea). Deionized (DI) water was obtained using a water deionizer (HUMAN POWER, Human Co., Seoul, Korea). All chemicals were used without further purification in this work.

2.2. Fabrication of PVDF Membranes

To begin, PVDF solutions of different concentrations were prepared by dissolving PVDF powder and LiCl in DMF solvent and stirring at 300 rpm for 3 h at 80 °C [40], then the solution was stood for 24 h to remove air bubbles. The prepared PVDF solution was transferred on a flat glass plate. A casting machine (motorized film applicator, Elcometer Inc., Manchester, UK) and casting knives (casting knife film applicator, Elcometer Inc., Manchester, UK) were used to control the thickness of the covered film at 300 µm. The covered film solution was immediately soaked in a coagulation bath containing DI water and/or EtOH for 1 h. As the final step, the membrane was placed in an oven at 60 °C for 24 h to obtain a dried, flat-sheet of membrane. By varying the compositions of the PVDF solution and the non-solvents, 7 different PVDF membranes were fabricated. The conditions of the membrane fabrication are summarized in Table 1.

Table 1. Experimental conditions for membrane fabrication.

Membrane Sample	PVDF Concentration [*w*/*w*]	LiCl Concentration [*w*/*w*]	Solvent	Non-Solvent [*v*/*v*]
S1	14.0%	0.0%	DMF	Water (100%)
S2	14.0%	3.0%	DMF	Water (100%)
S3	16.0%	3.0%	DMF	Water (100%)
S4	18.0%	3.0%	DMF	Water (100%)
S5	16.0%	3.0%	DMF	Water (90%) + EtOH (10%)
S6	16.0%	3.0%	DMF	Water (80%) + EtOH (20%)
S7	16.0%	3.0%	DMF	Water (70%) + EtOH (30%)

2.3. Contact Angle (CA) Measurement

The technique of sessile drop contact angle measurement was applied to the fabricated membranes as previously reported [11,40]. An instrument to measure the contact angle (Smart Drop) was supplied by Femtobiomed (Gyeonggi-do, Korea). The following procedures were used: (1) Membrane samples were placed on a plate; (2) water droplets (5 µL) were placed onto the membrane surface; (3) after the stabilization, the camera in the device captured images of the droplet from five different positions; and (4) the image analysis software connected to the instrument automatically determined the CA from the images. The measurements were repeated at least seven times per membrane sample and the average and standard deviation were recorded.

2.4. Measurement of Liquid Entry Pressure

An in-house apparatus was used to measure the liquid entry pressure (LEP) of the fabricated membranes [11,40]. As shown in Figure 1, the apparatus consists of an LEP chamber, a pressure gauge, a high-pressure N_2 gas cylinder, and a pipe. To begin, 50 mL DI water was poured into the chamber and a dried membrane sample was mounted. The chamber was then pressurized from its bottom using the N_2 gas cylinder connected with the pipe. The pressure was controlled using the gauge to determine the minimum pressure that resulted in the first water drop on the membrane surface. The LEP measurements were repeated three times and the average and the standard deviation were recorded.

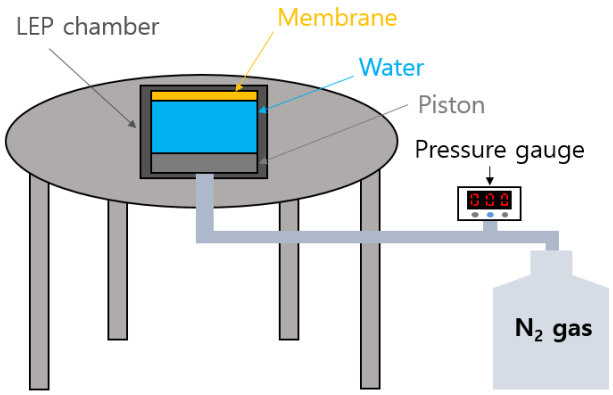

Figure 1. Schematic drawing of LEP apparatus.

2.5. Analysis of Membrane Morphology

A FE-SEM (FE-SEM 7800F Prime, JEOL Ltd., Tokyo, Japan) instrument was used for observing the microstructures of the prepared membranes as previously reported [41]. Before the analysis, the membrane samples were completely dried at 60 °C for 2 h in a drying oven. Then they were coated with platinum for 30 s by sputtering.

Atomic Force Microscope (AFM) was applied for an in-depth analysis of membrane surface. An AFM instrument (AFM, Atomic Force microscope, XE-100, PSIA Inc., Gyeonggi-do, Korea) was used to obtain the images. Based on the measurement results, the arithmetical mean deviation (R_a), root mean square deviation (R_q), and the vertical distance between the highest peak and lowest valley (R_{max}) were calculated using the same scan size (5 μm × 5 μm).

2.6. Analysis of Pore Size Distribution and Thickness Measurement

A capillary flow porometer (CFP-1500-AFL, porous materials Inc., Ithaca, New york, USA) was employed to measure the pore size distribution of the membranes [40]. Prior to the analysis, the membrane samples were soaked into the Galwick solution (porous materials Inc., Ithaca, New york, USA, surface tension = 15.9 dynes/cm), then N_2 gas was applied to the wetted membrane samples to obtain raw data required for the calculation of the pore size distribution of the membranes. The mean pore diameter (d_{mean}), maximum pore diameter (d_{max}), and the minimum pore diameter (d_{min}) were also estimated. The thickness of the membranes was measured using digital vernier calipers (Mitutoyo Inc., Kawasaki, Japan). At least three different locations on each sample were selected and analyzed to confirm the uniformity of the membranes, and the average and standard deviation were provided.

2.7. Measurement of Porosity

The gravimetric method was adopted to estimate the porosity of the membranes [42]. First, the membrane samples of equal size (2 × 2 cm^2) were immersed in ethanol. Second, the weights of the samples before and after saturation with ethanol were compared. Using the measured data, the membrane porosity (ε) was calculated:

$$\varepsilon = \frac{(m_1 - m_2)/D_e}{\left[(m_1 - m_2)/D_e + m_2/D_p\right]} \quad (1)$$

where m_1 is the mass of the saturated membrane (g), m_2 is the mass of the dry membrane (g), D_e is the specific gravity of the ethanol (g/cm^3), and D_p is the specific gravity of the PVDF material (g/cm^3).

2.8. Measurement of Flux and Rejection

The flux and salt rejection of the membranes were determined by carrying out a set of direct contact membrane distillation (DCMD) experiments. The schematic diagram

of the DCMD set-up is illustrated in Figure 2. Details on this technique were previously reported [40,41] and only a slight modification was done in this work. The effective membrane area was 12 cm^2. The initial volumes of the feed and the permeate were 2.0 L and 1.0 L, respectively. The feed and permeate temperatures were fixed at 60 ± 1.5 °C and 20 ± 1.5 °C, respectively, which were controlled using a heater and a chiller. The flow rates of the feed and permeate were 0.7 L/min and 0.4 L/min, respectively. Moreover, the feed and permeate pressures were measured to be 0.08 bar and 0.02 bar, respectively.

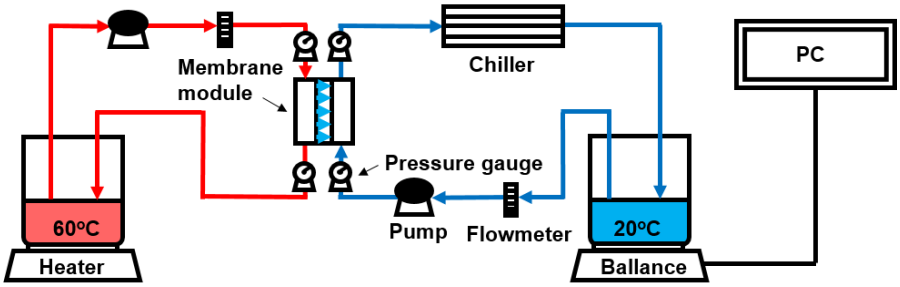

Figure 2. Schematic diagram of an equipment for DCMD experiments.

The feed solution was 35 g/L NaCl solution and the permeate solution was the DI water. The electrical conductivity of the feed and permeate was measured using a conductivity meter (WTW multi 3420, WTW, Munich, Germany). The conductivity was converted to the concentration using a standard curve [11,41]. The weight of the permeate tank was periodically measured using an electronic balance (Explorer Pro, Ohaus, Newark, NJ, USA) and the flux was calculated based on the following equation [13,43]:

$$J_v = \frac{\Delta m_g}{A_m \Delta t} \quad (2)$$

where Δm_g is the increased mass of the permeate, A_m is the membrane areas, and Δt is the time interval. The apparent salt rejection (R_{app}) was calculated by [44]:

$$R_{app} = 1 - \frac{c_p}{c_{f,0}} \quad (3)$$

where $c_{f,0}$ is the initial feed concentration, and the c_p is the permeate concentration. It should be noted that the intrinsic rejection (R_{int}) is different from the apparent rejection in the DCMD operation. Accordingly, R_{app} may be misleading because it generally overestimates the rejection capability of the membrane. The technique to calculate R_{int} from R_{app} will be discussed later.

2.9. Calculation of Additional Membrane Properties

The flux, rejection, contact angle (CA), liquid entry pressure (LEP), and pore sizes are primary properties of MD membranes. However, they are not sufficient to understand the complicated trade-offs of MD membrane performances. The flux and rejection are apparent properties and affected by the operating conditions. The CA and LEP cannot be directly correlated if the membrane morphology is complex. Accordingly, a set of equations were derived and used to evaluate additional (secondary) properties, including water vapor permeability (B_w), salt leakage ratio (L_w), and fiber radius (R_f).

2.9.1. Calculation of Water Vapor Permeability (B_w)

The water vapor transport in the DCMD process is driven by the difference in the vapor pressure between both sides of the membrane. The dependence of the water flux (J_v) on the vapor pressure difference (Δp_w) is described by [18,19]:

$$J_v = B_w \Delta p_w = B_w (p^0_{w,f} a_{w,f} - p^0_{w,p} a_{w,p}) \approx B_w p^0_{w,f} a_{w,f} = B_w p^0_{w,f} \gamma_{w,f} x_{w,f} \quad (4)$$

where B_w is the water vapor permeability; p_w is the vapor pressure; a_w is the activity; γ is the activity coefficient; x_w is the mole fraction of water. The subscripts f and p refer to feed and permeate, respectively, and the superscript 0 refers to pure water. B_w is an intrinsic coefficient depending on the membrane properties such as pore diameter, porosity, and the length of the pores, but also affected by the applied temperature.

The vapor pressure of pure water is estimated by the Antoine equation [45]:

$$p^0_{w,f} = e^{(23.1964 - 3816.44/(T_f - 46.13))} \tag{5}$$

When NaCl is used to prepare the feed solution, the activity coefficient of the water in the feed ($\gamma_{w,f}$) is given as a function of the mole fraction of NaCl (x_{NaCl}) [16,45]:

$$\gamma_{w,f} = 1 - 0.5x_{NaCl} - 10x^2_{NaCl} \tag{6}$$

The mole fraction of the water in the feed is [16,45]:

$$x_{w,f} = 1 - x_{NaCl} \tag{7}$$

Combining the Equations (4)–(7), the B_w is calculated from experimentally-determined flux by use of:

$$B_w = \frac{J_v}{\left(e^{(23.1964 - 3816.44/(T_f - 46.13))}\right)(1 - 0.5x_{NaCl} - 10x^2_{NaCl})(1 - x_{NaCl})} \tag{8}$$

B_w corresponds to water permeability of a membrane in pressure-driven membrane processes such as MF, UF, and RO. Since it does not change by the feed concentration (i.e., x_{NaCl}), it may be used as an intrinsic property of a membrane.

2.9.2. Estimation of Salt Leakage Ratio (L_w)

The salt transport in the DCMD process (J_s) is attributed to two mechanisms: (1) the transfer of salts with the water vapor (distillation) and (2) the leakage of feed water through wetted pores. In theory, the distilled water does not contain any salts and the contribution of the first mechanisms is negligible. Accordingly, the following equation is obtained to calculate J_s:

$$J_s = \left(\frac{J_v}{\rho}\right)(1 - L_w)c_{p,distill} + \left(\frac{J_v}{\rho}\right)L_w c_{p,leak} \approx \left(\frac{J_v}{\rho}\right)L_w c_{p,leak} = \left(\frac{J_v}{\rho}\right)L_w c_f = \left(\frac{J_v}{\rho}\right)c_{p,net} \tag{9}$$

where L_w is the leakage ratio, which is defined as the ratio of water leakage to total permeate; ρ is the density of water, $c_{p,distill}$ is the salt concentration in the distilled water; $c_{p,leak}$ is the salt concentration in the water leakage; $c_{p,net}$ is the salt concentration of the water transferred through the membrane; c_f is the salt concentration in the feed. It should be noted that the $c_{p,net}$ is different from the apparent permeate concentration (c_p) since the water transferred through the membrane is mixed with the recirculated water in the permeate side. Accordingly, $c_{p,net} = L_w\, c_{p,leak} = L_w\, c_f \neq c_p$. This leads to a difference between the apparent rejection (R_{app}) and the intrinsic rejection (R_{int}), which is given by:

$$R_{\text{int}} = 1 - \frac{c_{p,net}}{c_f} = 1 - \frac{L_w c_f}{c_f} = 1 - L_w \tag{10}$$

In DCMD processes, the mass balances of the salt and the water can be established respectively as follows:

$$\frac{d(c_p V_p)}{dt} = \left(\frac{J_v}{\rho}\right)L_w c_f A_m \tag{11}$$

$$\frac{dV_p}{dt} = \left(\frac{J_v}{\rho}\right) A_m \tag{12}$$

Accordingly, the following equation is used to calculate L_w from the results of DCMD experiments:

$$L_w = \left(\frac{\rho}{J_v}\right) \frac{\frac{d(c_p V_p)}{dt}}{c_f A_m} = \frac{\frac{d(c_p V_p)}{dt}}{c_f \frac{dV_p}{dt}} \approx \frac{\frac{\Delta(c_p V_p)}{\Delta t}}{c_f \frac{\Delta V_p}{\Delta t}} \tag{13}$$

2.9.3. Determination of Fiber Radius (R_f)

The Young-Laplace model is a well-known equation to correlate LEP with contact angle. With the assumption of cylindrical pores, LEP is described by [46]:

$$\Delta P = \left(\frac{-2\gamma}{r}\right) \cos\theta \tag{14}$$

where ΔP is liquid entry pressure, γ is the surface tension of the feed solution, r is pore radius, and θ is the intrinsic contact angle between the liquid and the membrane material [47]. However, the Young-Laplace model does not reflect the effect of membrane surface morphologies and cannot explain positive LEP values for membranes with θ less than 90°, which have been reported in the literature. In this case, the Purcell model (Figure 3) should be applied instead of the Young-Laplace model since it allows the prediction of positive LEP for membranes with relatively small contact angle. The equation for LEP in the Purcell model is given by [47,48]:

$$\Delta P = \left(\frac{-2\gamma}{r}\right) \frac{\cos(\theta + \alpha)}{1 + \frac{R_f}{r}(1 - \cos(\alpha))} \tag{15}$$

$$\sin(\theta + \alpha) = \frac{\sin\theta}{1 + \frac{r}{R_f}} \tag{16}$$

where R_f is the fiber radius and α is the angle below horizontal in the fiber. The R_f is calculated by simultaneously solving Equations (15) and (16). It is worth noting that R_f is an important intrinsic property of the MD membranes. Although the surface properties are similar, the LEP of the membranes changes with different R_f values. In other words, the LEP, which is related to wetting resistance, is affected not only by the hydrophobicity of the material but also by morphological parameters such as R_f.

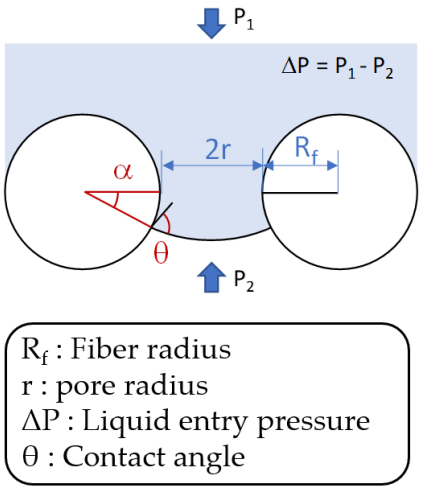

Figure 3. Interface in toroidal pore of hydrophobic membrane based on Purcell model.

3. Results and Discussion

3.1. Characterization of Fabricated Membranes

As indicated in Table 1, seven membranes were fabricated under different conditions. The PVDF concentration, LiCl concentration, and the composition of the non-solvent were varied. The surface and cross-sectional images of the prepared membranes were presented in Figures 4 and 5. As a common observation, all the membranes were asymmetric and showed both finger-like and sponge-like regions. Smaller pores seem to be formed in the membranes prepared without LiCl (S1, Figures 4a and 5a) than the other membranes. The addition of LiCl to the casting solution increased the rate of precipitation during the immersion step of phase inversion process, leading to the formation of a coarser structure of the membrane [39]. When the PVDF concentration increased from 14 wt.% to 18 wt.% in the presence of LiCl (S2, S3, S4, Figures 4b–d and 5b–d), the sizes of the finger-like structures were reduced as a result to the retardation of the phase separation rate [34,49]. On the other hand, the addition of EtOH to the non-solvent (S5, S6, S7, Figures 4e–g and 5e–g) decreased the sizes of the finger-like structures and enlarged the sponge-like regions. This is attributed to a reduction in the phase separation rate as an increase in the EtOH concentration [49]. The solubility parameter for PVDF and EtOH is smaller than that for the PVDF and water due to the effect of the hydrogen bonding [50], indicating that PVDF is more miscible with EtOH than water. Accordingly, a slower phase separation is expected in the presence of EtOH in the non-solvent.

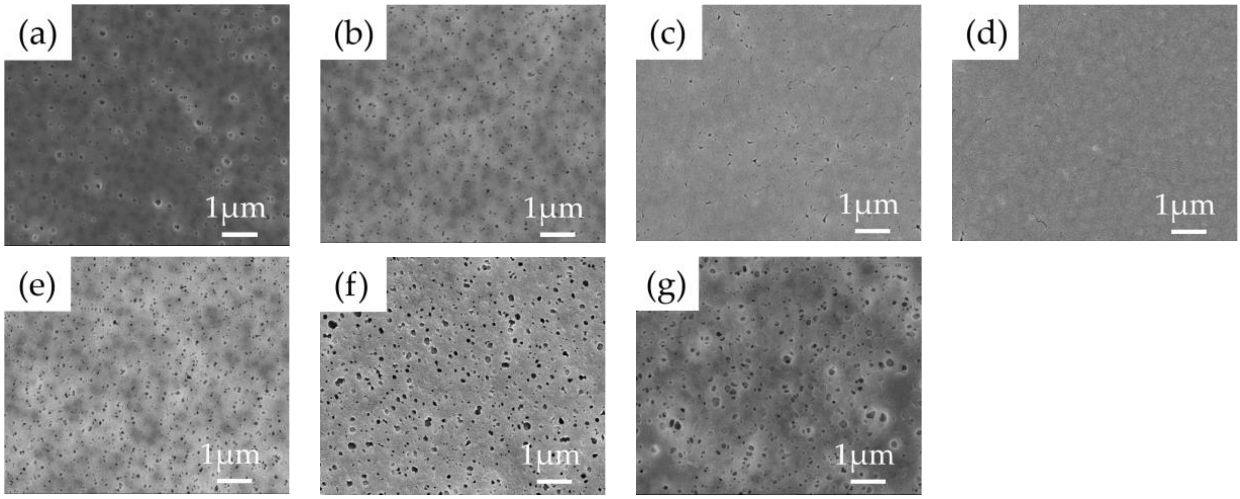

Figure 4. FE-SEM images of top surface of flat-sheet membranes with different PVDF, LiCl concentration and non-solvent compositions: (**a**) (S1) PVDF 14 wt.% with water, (**b**) (S2) PVDF 14 wt.% + LiCl with water, (**c**) (S3) PVDF 16 wt.% + LiCl with water, (**d**) (S4) PVDF 18 wt.% + LiCl with water, (**e**) (S5) PVDF 16 wt.% + LiCl with water (90%) + EtOH (10%), (**f**) (S6) PVDF 16 wt.% + LiCl with water (80%) + EtOH (20%) and (**g**) (S7) PVDF 16 wt.% + LiCl with water (70%) + EtOH (30%).

Table 2 summarizes the characteristics of the fabricated membranes. The contact angles of the fabricated membranes ranged between 75.1° and 90.3°. The addition of LiCl to the casting solution does not seem to significantly affect the contact angle (S1, S2). The contact angle did not increase with an increase in the PVDF concentration from 14.0 wt.% to 18.0 wt.% (S2, S3, S4). One the other hand, the contact angle increased by increasing the EtOH concentration in the non-solvent from 0 wt.% to 30 wt.% (S3, S5, S6, S7). Since the addition of EtOH instead of water retarded the rate of phase separation, the size of the polymer crystals increased as well as the surface roughness, thereby increasing the contact angle [26,39]. Although the contact angles were relatively small, the LEP values were higher than generally expected. According to the Young-Laplace equation, the membranes with the contact angle less than 90° should have negative LEP values. However, the LEP values for the fabricated membranes were measured in the range between 1.13 bar to

3.19 bar. Without LiCl, the LEP value was the highest (3.19 bar, S1), which is attributed to its dense structures. In the presence of LiCl, the LEP increased with an increase in the PVDF concentration (S2, S3, S4). It should be noted that the LEP values were different with similar values of the contact angle in these cases. As the EtOH concentration in the non-solvent increased, the LEP increased and then decreased (S3, S5, S6, S7). Again, the LEP and contact angle did not exhibit a strong correlation.

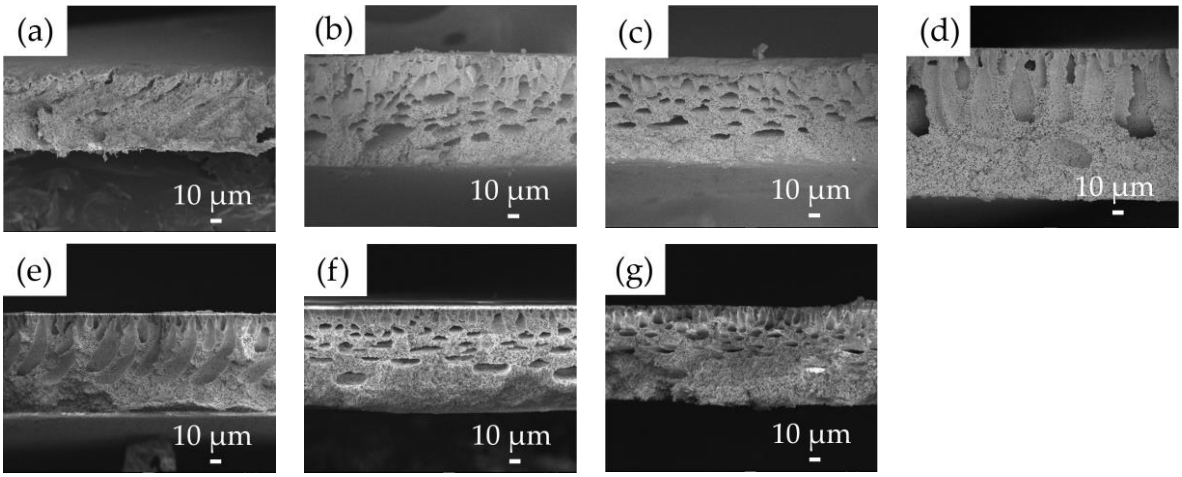

Figure 5. FE-SEM images of cross-section of flat-sheet membranes with different PVDF, LiCl concentration and non-solvent compositions: (**a**) (S1) PVDF 14 wt.% with water, (**b**) (S2) PVDF 14 wt.% + LiCl with water, (**c**) (S3) PVDF 16 wt.% + LiCl with water, (**d**) (S4) PVDF 18 wt.% + LiCl with water, (**e**) (S5) PVDF 16 wt.% + LiCl with water (90%) + EtOH (10%), (**f**) (S6) PVDF 16 wt.% + LiCl with water (80%) + EtOH (20%) and (**g**) (S7) PVDF 16 wt.% + LiCl with water (70%) + EtOH (30%).

Table 2. Primary (measurable) properties of fabricated membranes.

Membrane Sample	Contact Angle (°)	LEP (bar)	Membrane Thickness (μm)	Porosity (%)	d_{mean} (μm)	d_{max} (μm)	d_{min} (μm)
S1	76.9 ± 3.3	3.19 ± 0.57	68.0 ± 3.4	85.4 ± 2.5	0.09	0.13	0.07
S2	75.1 ± 1.1	1.13 ± 0.09	80.3 ± 3.3	88.3 ± 2.3	0.17	0.29	0.12
S3	75.7 ± 1.7	1.77 ± 0.23	85.2 ± 6.4	85.2 ± 2.0	0.18	0.28	0.08
S4	76.9 ± 1.9	1.87 ± 0.14	98.8 ± 3.0	84.9 ± 1.3	0.16	0.26	0.10
S5	77.4 ± 2.8	2.45 ± 0.18	78.3 ± 2.4	86.1 ± 4.2	0.15	0.21	0.08
S6	83.6 ± 2.1	2.29 ± 0.06	79.7 ± 7.5	81.9 ± 1.5	0.16	0.25	0.08
S7	90.3 ± 3.6	2.08 ± 0.07	76.8 ± 0.8	83.6 ± 1.1	0.19	0.31	0.08

As presented in Table 2, the membrane thickness varied in the range from 68.0 μm to 98.8 μm. The thinnest membrane was obtained in the absence of LiCl (S1) while the thickest membrane was prepared with the highest PVDF concentration (S4). In the other cases, the thickness values were similar. The porosity of the membranes ranged from 81.9% to 88.3%. Although the morphologies of the membranes were different as shown in Figures 4 and 5, the porosities were not significantly different. This suggests that the size and shape of the void space in the membranes are different even with the similar porosity.

The mean (average), maximum, and minimum diameters of the pores in the membranes are presented in Table 2. The mean pore diameter of the membrane prepared without LiCl (S1) was 0.09 μm, which was the smallest. The mean pore size increased after adding LiCl. Moreover, the maximum and minimum pore diameters showed an increment by up to 2.38 times (S7) and 1.71 times (S2), respectively. As presented in Figure 6a, the pore size distribution shifted to the right by adding LiCl. However, no evident dependence of the pore size distribution on the PVDF concentration was observed. With an increase in the EtOH concentration from 10 wt.% to 30 wt.%, the pore size distribution moved to the right, as illustrated in Figure 6b.

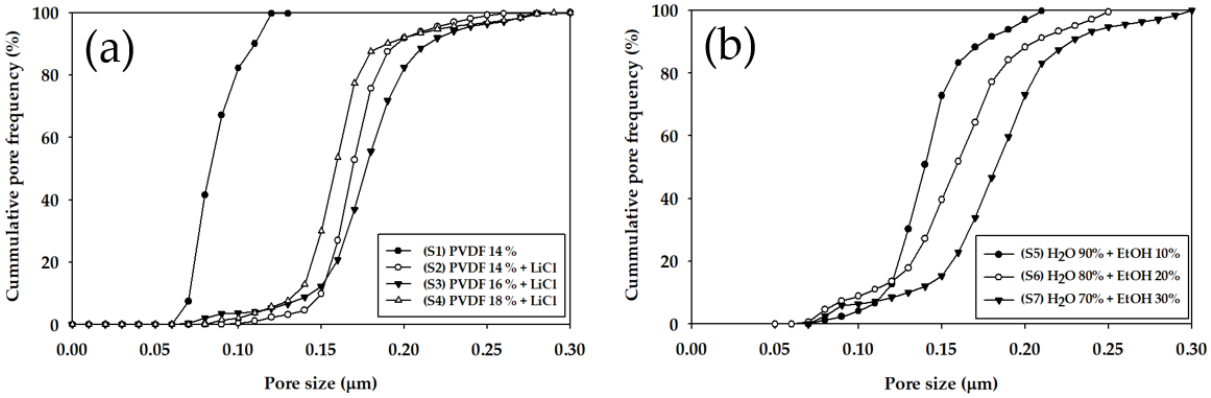

Figure 6. Cumulative pore frequency versus pore size of the membranes with different PVDF, LiCl concentration and non-solvent compositions: (**a**) (S1) PVDF 14 wt.% with water, (S2) PVDF 14 wt.% + LiCl with water, (S3) PVDF 16 wt.% + LiCl with water, and (S4) PVDF 18 wt.% + LiCl with water; (**b**) (S5) PVDF 16 wt.% + LiCl with water (90%) + EtOH (10%), (S6) PVDF 16 wt.% + LiCl with water (80%) + EtOH (20%), and (S7) PVDF 16 wt.% + LiCl with water (70%) + EtOH (30%).

3.2. DCMD Performance

Using the prepared membranes, a set of DCMD experiments were carried out in the experimental set-up (shown in Figure 2). The results are presented in Figure 7. The black symbols indicate the permeate flux and the red ones point out the permeate concentration of NaCl. Each DCMD experiment was carried out for 24 h. As shown in Figure 7a, the membrane prepared without LiCl (S1) resulted in a flux less than 6 kg/m^2-h and a permeate concentration less than 6 mg/L. The fabrication of the membranes in the presence of LiCl (S2, S3, and S4) substantially increased both the flux and permeate concentration. When the PVDF concentration was 14 wt.%, the increasing rate of the permeate concentration was the highest (Figure 7b). This is attributed to the fact that S2 had a wide pore size distribution and low LEP as shown in Table 2. A lower LEP may be related to a higher probability of salt passage, leading to higher permeate concentration. It gradually decreased with an increase in the PVDF concentration (Figure 7c,d). The increased concentration of EtOH in the non-solvent (S5, S6, S7) also affected the flux and permeate concentration as presented in Figure 7e–g.

The average flux and the apparent rejection in the DCMD experiments are summarized in Table 3. It is evident that there is a trade-off between flux and rejection. The membrane with the highest rejection showed the lowest flux (S1) while the membrane with the highest flux exhibited the lowest rejection (S2). Nevertheless, there was also an exception that allows relatively high flux and rejection simultaneously (S5, S7). Figure 8 gives an overview of the effect of fabrication conditions on the flux and rejection of the MD membranes. Since the focus of this work is not on the optimization of the membrane fabrication, the performance of these membranes such as flux and rejection may not be optimized. Nevertheless, it should be noted that the properties of the membranes are sensitive to their fabrication conditions, leading to different performances. Accordingly, an in-depth analysis to understand the relations among the membrane properties is required.

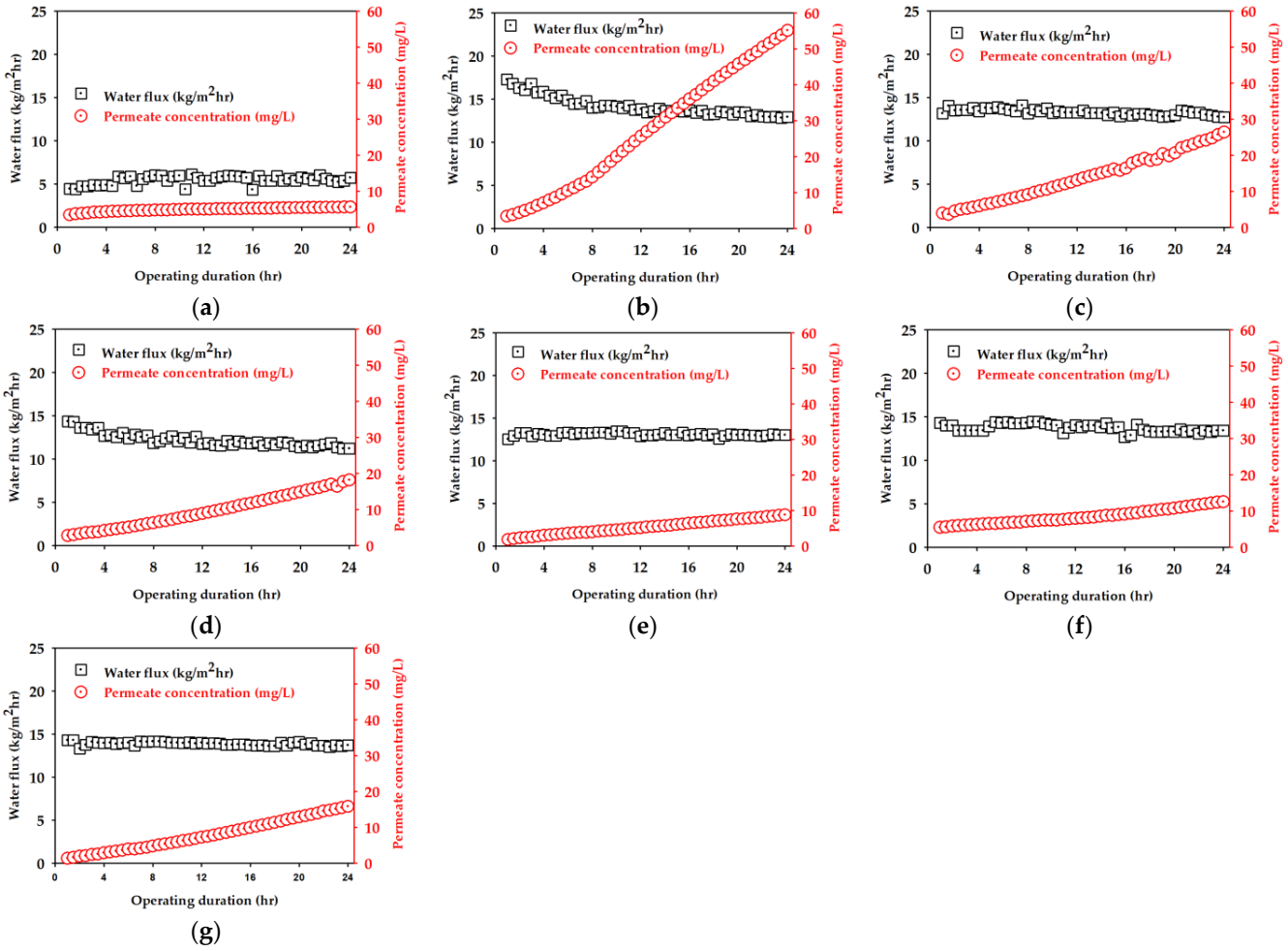

Figure 7. Water flux and salt permeate concentration for 24 h operation by DCMD on 35 g/L NaCl solution: (**a**) (S1) PVDF 14 wt.% with water, (**b**) (S2) PVDF 14 wt.% + LiCl with water, (**c**) (S3) PVDF 16 wt.% + LiCl with water, (**d**) (S4) PVDF 18 wt.% + LiCl with water, (**e**) (S5) PVDF 16 wt.% + LiCl with water (90%) + EtOH (10%), (**f**) (S6) PVDF 16 wt.% + LiCl with water (80%) + EtOH (20%), and (**g**) (S7) PVDF 16 wt.% + LiCl with water (70%) + EtOH (30%). For all DCMD experiments, the feed and distillate temperatures were 60 and 20 °C, respectively.

Table 3. Average water flux and apparent rejection for 24 h operation by DCMD on 35 g/L NaCl solution.

Membrane Sample	Flux (kg/m^2-h)	Apparent Rejection (%)
S1	5.45 ± 0.50	99.95 ± 0.005
S2	14.19 ± 1.14	99.75 ± 0.146
S3	13.32 ± 0.33	99.87 ± 0.061
S4	12.21 ± 0.78	99.91 ± 0.0043
S5	13.11 ± 0.19	99.95 ± 0.019
S6	13.73 ± 0.46	99.92 ± 0.0190
S7	13.87 ± 0.21	99.93 ± 0.041

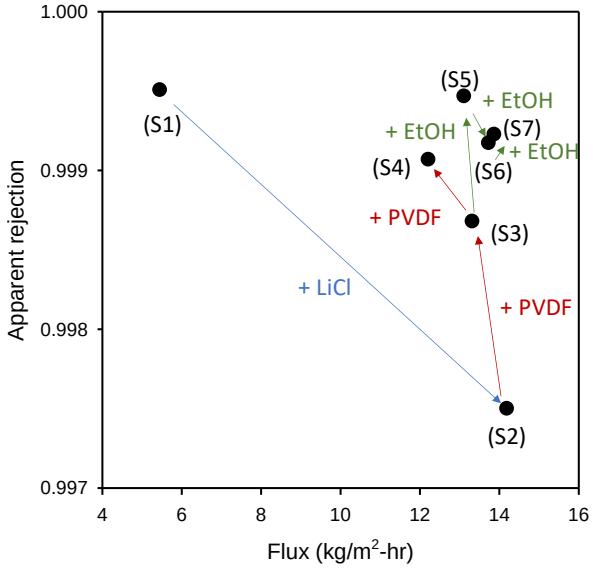

Figure 8. Changes in flux and apparent rejection with membrane fabrication conditions: An overview.

3.3. In-Depth Analysis of Membrane Properties

To further investigate the characteristics of the MD membranes, the "secondary" properties were calculated using the Equations (8), (13), (15), and (16). The results are presented in Table 4.

Table 4. Secondary (evaluated) properties of fabricated membranes.

Membrane Sample	Water Vapor Permeability, B_w ($\times 10^{-8}$ s/m)	Salt Leakage Ratio, L_w (-)	Fiber Radius, R_f (μm)
S1	7.76 ± 0.71	0.0020 ± 0.0019	0.598
S2	20.19 ± 1.62	0.0151 ± 0.0043	1.690
S3	18.96 ± 0.47	0.0073 ± 0.0049	0.938
S4	17.38 ± 1.11	0.0054 ± 0.0033	0.936
S5	18.66 ± 0.27	0.0024 ± 0.0006	0.714
S6	19.54 ± 0.65	0.0026 ± 0.0010	0.975
S7	19.74 ± 0.30	0.0045 ± 0.0012	1.503

The average water vapor permeability (B_w) ranged from 7.76 s/m to 20.19 s/m. As expected, a membrane with a high flux showed a high B_w. The salt leakage ratio (L_w) was observed in the range from 0.0020 to 0.0151. A membrane having a high rejection resulted in a low L_w. Since B_w and L_w are less dependent on the experimental conditions (i.e., feed concentration, MD operation time) than flux and rejection, they may be used as intrinsic properties of a membrane. Nevertheless, care should be taken because they may be also affected by the conditions such as feed temperatures.

Table 4 also presents fiber radius (R_f), which is related with the morphology of the membranes. Membranes prepared by the phase inversion technique often have pores consisting of the spaces between individual membrane fibers. R_f is the radius of the membrane fibers. In the Equations (15) and (16), LEP decreases as an increase in R_f if all the other conditions are the same. This suggests that membranes with the same pore size and hydrophobicity may have different LEP due to different R_f values. The R_f value of the membranes was calculated in the range from 0.598 μm to 1.690 μm.

3.4. Correlations among Different Properties

As the next step, the correlations between different membrane properties were investigated to explore the way to fabrication of efficient MD membranes. Figure 9a reveals the relationship between B_w and L_w. As expected, an increase in B_w resulted in an increase in

L_w, indicating a trade-off between the two properties. This is attributed to the fact that the membranes with higher B_w values have larger pore sizes. As presented in Figure 9b, the mean pore radius increased with an increase in B_w. Since L_w is related to the partial pore wetting, the membranes with larger pore sizes may have higher L_w values. The dependence of R_f on B_w is presented in Figure 9c. It is evident the R_f increases with an increase in B_w, implying that it is difficult to obtain membranes with high B_w and small R_f. This is probably because the membranes with large R_f may have larger pores due to their coarse structures.

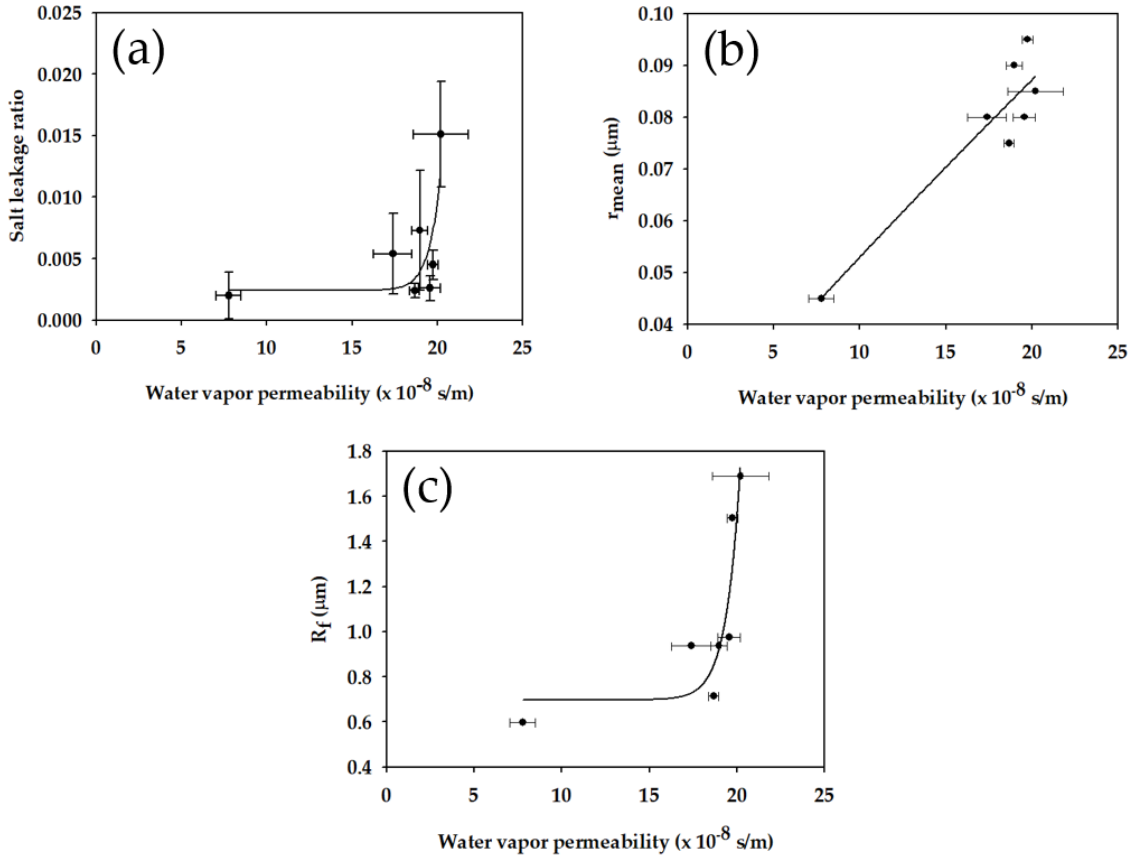

Figure 9. Effect of water vapor permeability (B_w) on (**a**) salt leakage ratio (L_w); (**b**) mean pore radius; (**c**) fiber radius (R_f) of fabricated membranes.

To provide insight into the factors affecting LEP, the effect of contact angle and pore size on LEP was further analyzed. As presented in Figure 10a, there was no correlation between the contact angle and LEP. Although LEP is affected by chemical properties represented by the contact angle, it is also a function of physical properties such as surface morphology. At least in our case, the latter seems to be more important than the former. On the other hand, the LEP is inversely proportional to the pore diameters as shown in Figure 10b. Not only the maximum pore diameter (d_{max}) but also the mean pore diameter (d_{mean}) and minimum pore diameter (d_{min}) showed reasonable correlations. A reduction in LEP by an increased pore size can be explained by the Equations (15) and (16).

As mentioned before, it is desired to obtain membranes with high B_w (or high flux) and high LEP. Based on the Equations (15) and (16), LEP increases with an increase in pore size and a decrease in R_f. Accordingly, the control of R_f may be a novel approach to increase LEP without sacrificing flux. Unfortunately, it seems that there is also a trade-off between the pore size and R_f. As presented in Figure 11, R_f increased as the pore size increased. This is probably because small membrane fibers are required to form small pores. Nevertheless, a further investigation is recommended to explore the method to increase the pore size and decrease R_f simultaneously.

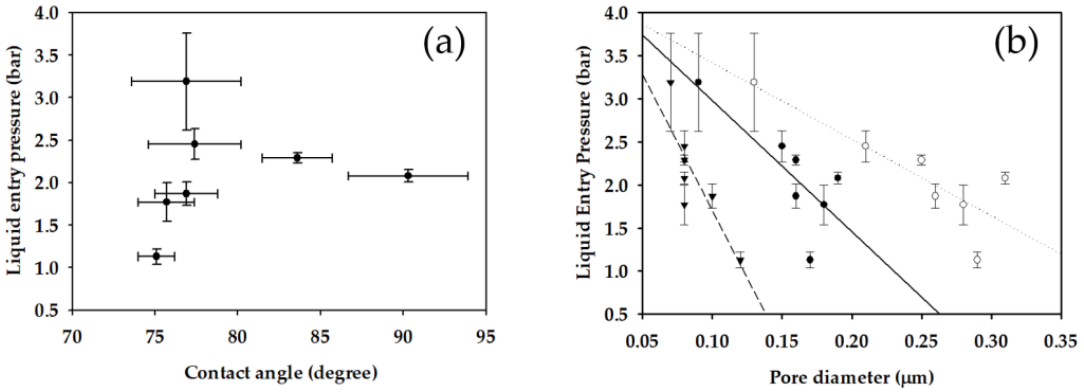

Figure 10. Exploration of factors affecting LEP of fabricated membranes: (**a**) Contact angle; (**b**) pore diameters (▼: minimum pore diameter; ●: mean pore diameter; ○: maximum pore diameter).

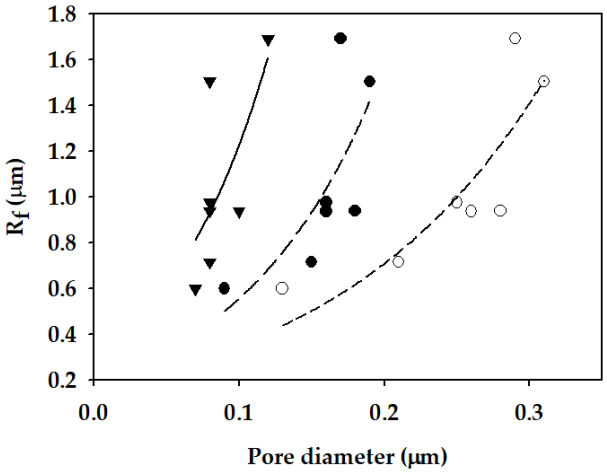

Figure 11. Dependence of R_f on pore sizes of fabricated membranes (▼: minimum pore diameter; ●: mean pore diameter; ○: maximum pore diameter).

Although R_f cannot be directly measured, it may be related to measurable properties of the membranes. To explore the possibility, AFM analysis was performed to determine the surface roughness parameters, which are used to correlate with R_f. The 3-D surface images of membranes are presented in Figure 12. Using the images, the arithmetical mean deviation (R_a), root mean square deviation (R_q), and vertical distance between highest peak and lowest valley (R_{max}) were calculated and summarized in Table 5. As a general observation, the roughness parameters increased with an increase in the EtOH concentration. Although S3 (0 wt.%) and S5 (10 wt.%) showed similar roughness parameters, S6 (20 wt.%) and S7 (30 wt.%) clearly exhibited higher values of the roughness parameters. This may be attributed to the occurrence of solid-liquid demixing (crystallization) in the presence of EtOH.

Figure 13 presents the dependence of the roughness parameters on R_f. There are increasing tendencies of the roughness parameters on R_f, suggesting that R_f may be related to the measurable properties. It is also plausible that an increase in R_f increases the surface roughness due to an increase in the distance between highest peak and lowest valley on the membrane surface.

Table 6 lists membrane properties between the current work and the previous investigation [40]. Although the contact angle of the commercial PVDF membrane was the highest (126°), the LEP was the lowest among these membranes. This is attributed to the fact that its pore size is the largest. The M1 and M2 membranes showed low contact angles but their LEP values were high due to their relatively small pore size as well as small R_f values. On the other hand, the S6 and S7 membranes showed moderate contact angles and

high LEP values. The apparent rejection of all membranes was similar, but the salt leakage ratio was different, ranging from 0.0015 (M1) to 0.0045 (S7). The R_f ranged from 0.350 (M2) to 1.503 (S7) membranes.

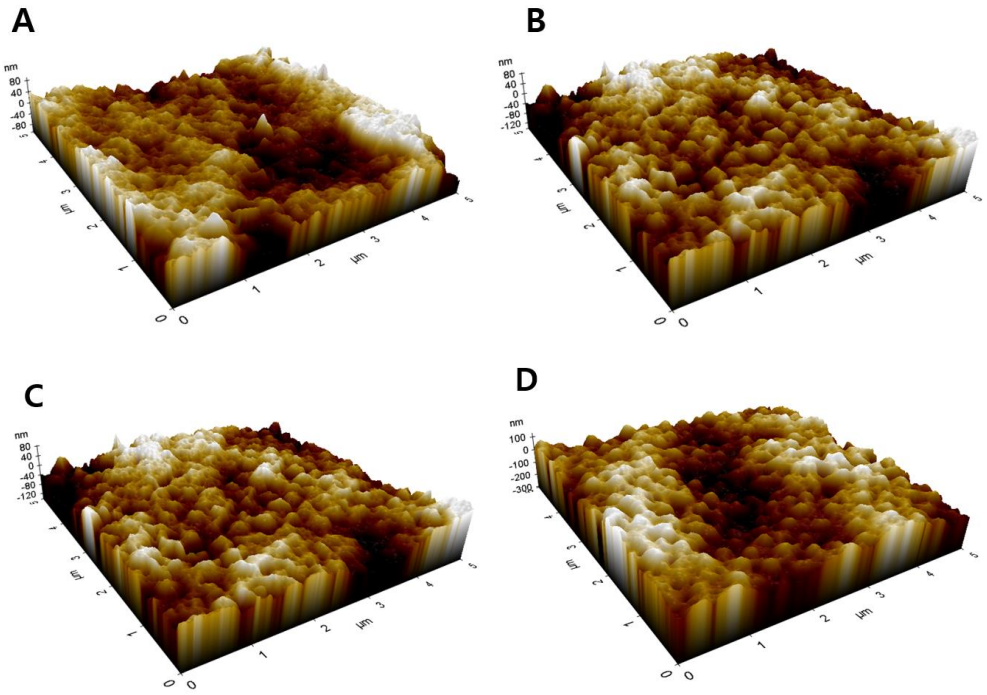

Figure 12. AFM images of fabricated membranes: (**A**) (S3) Water; (**B**) (S5) Water (90%) + EtOH (10%); (**C**) (S6) Water (80%) + EtOH (20%); and (**D**) (S7) Water (70%) + EtOH (30%).

Table 5. Roughness parameters of the prepared membranes.

Membrane Sample	R_a (nm) [a]	R_q (nm) [b]	R_{max} (nm) [c]
S3	20.01	25.47	89.87
S5	18.51	23.97	83.49
S6	27.03	34.09	103.22
S7	40.80	51.13	129.44

[a] R_a (nm): Arithmetical mean deviation. [b] R_q (nm): Root mean square deviation. [c] R_{max} (nm): Vertical distance between highest peak and lowest valley.

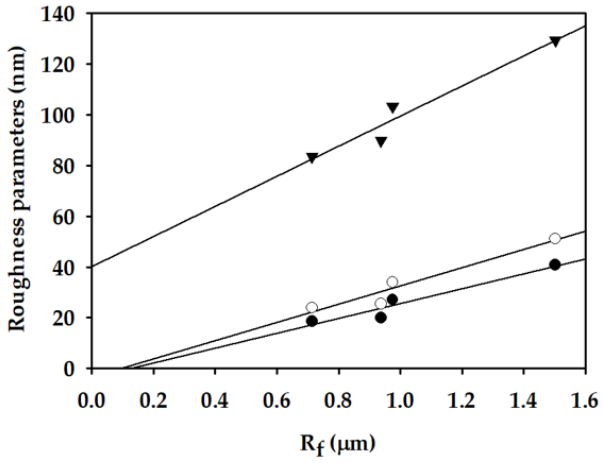

Figure 13. Roughness parameters versus Fiber radius of fabricated membranes (●: arithmetical mean deviation (R_a); ○: root mean square deviation (R_q); ▼: vertical distance between highest peak and lowest valley (R_{max}).

Table 6. Comparison of the membrane properties obtained in this study with the literature for DCMD process.

Membrane Sample	Contact Angle (°)	LEP (bar)	d_{mean} (µm)	Flux (kg/m^{2}h)	Apparent Rejection (%)	Water Vapor Permeability, B_w, ($\times 10^{-8}$ s/m)	Salt Leakage Ratio, L_w (-)	Fiber Radius, R_f (µm)
S6	83.6 ± 2.1	2.29 ± 0.06	0.16	13.73 ± 0.46	99.92 ± 0.0190	19.54 ± 0.65	0.0026 ± 0.0010	0.975
S7	90.3 ± 3.6	2.08 ± 0.07	0.19	13.87 ± 0.21	99.93 ± 0.0410	19.74 ± 0.30	0.0045 ± 0.0012	1.503
M1 [40]	75.7 ± 1.4	2.93 ± 0.06	0.11	20.20 ± 0.10	99.93 ± 0.0182	28.73 ± 0.27	0.0015 ± 0.0003	0.618
M2 [40]	73.2 ± 2.7	4.16 ± 0.25	0.07	8.6 ± 0.11	99.93 ± 0.0145	12.26 ± 0.12	0.0026 ± 0.0007	0.350
Commercial PVDF [40]	126.8 ± 1.1	1.81 ± 0.16	0.22	15.10 ± 0.61	99.93 ± 0.0087	21.69 ± 0.65	0.0023 ± 0.0009	0.429

4. Conclusions

This study presents an approach to evaluate the properties of MD membranes using seven PVDF membranes synthesized under different conditions. The following conclusions were drawn based on the findings:

1. Depending on the fabrication conditions, membranes with flux, rejection, contact angle (CA), liquid entry pressure (LEP), and pore sizes were obtained. Without LiCl, a membrane with small pore size, high LEP and low flux was prepared. When LiCl was used, an increase in PVDF concentration led to the formation of denser membranes. The flux and rejection were further adjusted by controlling the EtOH concentration in the non-solvent.
2. Using the equations derived in this work, B_w, L_w, and R_f were calculated. It was found that B_w and L_w ranged from 7.76×10^{-8} s/m to 20.19×10^{-8} s/m and from 0.0020 to 0.0151, respectively. An increase in B_w resulted in an increased L_w, indicating a trade-off between the two properties. This is attributed to the fact that the membranes with higher B_w values have larger pore sizes.
3. R_f was calculated in the range from 0.598 μm to 1.690 μm. Since the R_f was relatively small, the prepared membranes can have high LEP (more than 1.13 bar) even at low CA (less than 90.8°). R_f was found to be correlated with the surface roughness measured by AFM.
4. An efficient MD membrane should have a high flux, rejection, and LEP with low fouling propensity. The results in this study suggest that the pore size should be high to ensure high B_w but R_f should be small to lower L_w. However, care should be taken in this approach. Since there is a trade-off between pore size and R_f, it may not be possible to simultaneously increase both properties. In addition, an increase in the pore size above a critical value is not allowed due to high risk of the wetting.
5. If R_f is sufficiently small, it is plausible to fabricate membranes using moderately hydrophobic materials, which is beneficial to retard fouling due to hydrophobic foulants. Nevertheless, further work should be done to examine this hypothesis.

Author Contributions: Conceptualization, M.A. and S.L. (Sangho Lee); Investigation, M.A., S.L. (Sangho Lee), H.C. and Y.C.; Methodology, M.A. and S.L. (Sangho Lee); Supervision, S.L. (Sangho Lee); Writing—original draft preparation, M.A. and S.L. (Sangho Lee); Writing—review and editing, M.A., S.L. (Sangho Lee), H.C. and S.L. (Seockheon Lee). All authors have read and agreed to the published version of the manuscript.

Funding: This study was funded by the National Research of Korea (NRF-2021R1A2C1013611).

Institutional Review Board Statement: Not applicable.

Informed Consent Statement: Not applicable.

Data Availability Statement: Not applicable.

Acknowledgments: This study was supported by the National Research of Korea (NRF-2021R1A2C1-013611). The authors thank Jaehyun Ju and Jihyeok Choi for their continued support in encouraging and improving the quality of the paper.

Conflicts of Interest: The authors declare no conflict of interest.

Abbreviations

A_m	membrane area (m^2)
a_w	activity of water (-)
B_w	water vapor permeability (s/m)
c_f	salt concentration in the feed (kg/m^3)
$c_{f,0}$	initial feed concentration (kg/m^3)
c_p	permeate concentration (kg/m^3)

$c_{p,distill}$	salt concentration in the distilled water (kg/m^3)
$c_{p,leak}$	salt concentration in the water leakage (kg/m^3)
$c_{p,net}$	salt concentration of the water transferred through the membrane (kg/m^3)
D_e	specific gravity of the ethanol (g/cm^3)
D_p	specific gravity of the PVDF material (g/cm^3)
J_v	permeate (water) flux (kg/m^2-h)
L_w	leakage ratio (-)
m_1	mass of the saturated membrane (g)
m_2	mass of the dry membrane (g)
p_w	vapor pressure (bar)
R_{app}	apparent salt rejection (-)
R_{int}	intrinsic rejection (-)
subscript f	feed
subscript p	permeate
superscript 0	pure water
x_{NaCl}	mole fraction of NaCl (-)
x_w	mole fraction of water (-)
Δm_g	increased mass of the permeate (g)
Δp_w	vapor pressure difference (bar)
Δt	time interval (s)
γ	activity coefficient (-)
$\gamma_{w,f}$	activity coefficient of water in the feed (-)
ρ	density of water (kg/m^3)

References

1. Lu, S.; Bai, X.; Li, W.; Wang, N. Impacts of climate change on water resources and grain production. *Technol. Forecast. Soc. Chang.* **2019**, *143*, 76–84. [CrossRef]
2. Zhuang, X.W.; Li, Y.P.; Nie, S.; Fan, Y.R.; Huang, G.H. Analyzing climate change impacts on water resources under uncertainty using an integrated simulation-optimization approach. *J. Hydrol.* **2018**, *556*, 523–538. [CrossRef]
3. Pistocchi, A.; Bleninger, T.; Breyer, C.; Caldera, U.; Dorati, C.; Ganora, D.; Millán, M.M.; Paton, C.; Poullis, D.; Herrero, F.S.; et al. Can seawater desalination be a win-win fix to our water cycle? *Water Res.* **2020**, *182*, 115906. [CrossRef]
4. Aziz, N.I.H.A.; Hanafiah, M.M. Application of life cycle assessment for desalination: Progress, challenges and future directions. *Environ. Pollut.* **2021**, *268*, 115948. [CrossRef] [PubMed]
5. Takabatake, H.; Taniguchi, M.; Kurihara, M. Advanced Technologies for Stabilization and High Performance of Seawater RO Membrane Desalination Plants. *Membranes* **2021**, *11*, 138. [CrossRef]
6. Suwaileh, W.; Johnson, D.; Hilal, N. Membrane desalination and water re-use for agriculture: State of the art and future outlook. *Desalination* **2020**, *491*, 114559. [CrossRef]
7. Ibrahim, Y.; Ismail, R.A.; Ogungbenro, A.; Pankratz, T.; Banat, F.; Arafat, H.A. The sociopolitical factors impacting the adoption and proliferation of desalination: A critical review. *Desalination* **2021**, *498*, 114798. [CrossRef]
8. Lee, S.; Choi, J.; Park, Y.-G.; Shon, H.; Ahn, C.H.; Kim, S.-H. Hybrid desalination processes for beneficial use of reverse osmosis brine: Current status and future prospects. *Desalination* **2019**, *454*, 104–111. [CrossRef]
9. Panagopoulos, A.; Haralambous, K.-J. Environmental impacts of desalination and brine treatment—Challenges and mitigation measures. *Mar. Pollut. Bull.* **2020**, *161*, 111773. [CrossRef] [PubMed]
10. Soliman, M.N.; Guen, F.Z.; Ahmed, S.A.; Saleem, H.; Khalil, M.J.; Zaidi, S.J. Energy consumption and environmental impact assessment of desalination plants and brine disposal strategies. *Process Saf. Environ. Prot.* **2021**, *147*, 589–608. [CrossRef]
11. Cho, H.; Choi, J.; Choi, Y.; Lee, S. Ultrasonic-assisted removal of inorganic scales in high-salinity wastewater treatment using membrane distillation. *Desalination Water Treat.* **2019**, *157*, 383–392. [CrossRef]
12. Panagopoulos, A.; Haralambous, K.-J.; Loizidou, M. Desalination brine disposal methods and treatment technologies—A review. *Sci. Total Environ.* **2019**, *693*, 133545. [CrossRef]
13. Choi, Y.; Naidu, G.; Lee, S.; Vigneswaran, S. Recovery of sodium sulfate from seawater brine using fractional submerged membrane distillation crystallizer. *Chemosphere* **2020**, *238*, 124641. [CrossRef]
14. Elcik, H.; Fortunato, L.; Alpatova, A.; Soukane, S.; Orfi, J.; Ali, E.; AlAnsary, H.; Leiknes, T.; Ghaffour, N. Multi-effect distillation brine treatment by membrane distillation: Effect of antiscalant and antifoaming agents on membrane performance and scaling control. *Desalination* **2020**, *493*, 114653. [CrossRef]
15. Drioli, E.; Ali, A.; Macedonio, F. Membrane distillation: Recent developments and perspectives. *Desalination* **2015**, *356*, 56–84. [CrossRef]
16. Alkhudhiri, A.; Darwish, N.; Hilal, N. Membrane distillation: A comprehensive review. *Desalination* **2012**, *287*, 2–18. [CrossRef]

17. Tijing, L.D.; Woo, Y.C.; Choi, J.-S.; Lee, S.; Kim, S.-H.; Shon, H.K. Fouling and its control in membrane distillation—A review. *J. Membr. Sci.* **2015**, *475*, 215–244. [CrossRef]
18. Ashoor, B.; Mansour, S.; Giwa, A.; Dufour, V.; Hasan, S. Principles and applications of direct contact membrane distillation (DCMD): A comprehensive review. *Desalination* **2016**, *398*, 222–246. [CrossRef]
19. Park, Y.; Lee, S. Analysis of thermal energy efficiency for hollow fiber membranes in direct contact membrane distillation. *Environ. Eng. Res.* **2019**, *24*, 347–353. [CrossRef]
20. Warsinger, D.M.; Swaminathan, J.; Guillen-Burrieza, E.; Arafat, H.A.; Lienhard, V.J.H. Scaling and fouling in membrane distillation for desalination applications: A review. *Desalination* **2015**, *356*, 294–313. [CrossRef]
21. Ahmed, F.E.; Lalia, B.S.; Hashaikeh, R.; Hilal, N. Alternative heating techniques in membrane distillation: A review. *Desalination* **2020**, *496*, 114713. [CrossRef]
22. Schwantes, R.; Chavan, K.; Winter, D.; Felsmann, C.; Pfafferott, J. Techno-economic comparison of membrane distillation and MVC in a zero liquid discharge application. *Desalination* **2018**, *428*, 50–68. [CrossRef]
23. Alsebaeai, M.K.; Ahmad, A.L. Membrane distillation: Progress in the improvement of dedicated membranes for enhanced hydrophobicity and desalination performance. *J. Ind. Eng. Chem.* **2020**, *86*, 13–34. [CrossRef]
24. Chew, N.G.P.; Zhao, S.; Wang, R. Recent advances in membrane development for treating surfactant-and oil-containing feed streams via membrane distillation. *Adv. Colloid Interface Sci.* **2019**, *273*, 102022. [CrossRef]
25. Guan, G.; Yang, X.; Wang, R.; Fane, A.G. Modular matrix design for large-scale membrane distillation system via Aspen simulations. *Desalination* **2018**, *428*, 207–217. [CrossRef]
26. Eykens, L.; De Sitter, K.; Dotremont, C.; Pinoy, L.; Van der Bruggen, B. Membrane synthesis for membrane distillation: A review. *Sep. Purif. Technol.* **2017**, *182*, 36–51. [CrossRef]
27. Tibi, F.; Charfi, A.; Cho, J.; Kim, J. Fabrication of polymeric membranes for membrane distillation process and application for wastewater treatment: Critical review. *Process Saf. Environ. Prot.* **2020**, *141*, 190–201. [CrossRef]
28. Lu, K.J.; Chen, Y.; Chung, T.-S. Design of omniphobic interfaces for membrane distillation–A review. *Water Res.* **2019**, *162*, 64–77. [CrossRef]
29. Afsari, M.; Shon, H.K.; Tijing, L.D. Janus membranes for membrane distillation: Recent advances and challenges. *Adv. Colloid Interface Sci.* **2021**, 102362. [CrossRef]
30. Fadhil, S.; Marino, T.; Makki, H.F.; Alsalhy, Q.F.; Blefari, S.; Macedonio, F.; Di Nicolò, E.; Giorno, L.; Drioli, E.; Figoli, A. Novel PVDF-HFP flat sheet membranes prepared by triethyl phosphate (TEP) solvent for direct contact membrane distillation. *Chem. Eng. Process. Process Intensif.* **2016**, *102*, 16–26. [CrossRef]
31. Woo, Y.C.; Kim, Y.; Shim, W.-G.; Tijing, L.D.; Yao, M.; Nghiem, L.D.; Choi, J.-S.; Kim, S.-H.; Shon, H.K. Graphene/PVDF flat-sheet membrane for the treatment of RO brine from coal seam gas produced water by air gap membrane distillation. *J. Membr. Sci.* **2016**, *513*, 74–84. [CrossRef]
32. Zheng, L.; Wu, Z.; Wei, Y.; Zhang, Y.; Yuan, Y.; Wang, J. Preparation of PVDF-CTFE hydrophobic membranes for MD application: Effect of LiCl-based mixed additives. *J. Membr. Sci.* **2016**, *506*, 71–85. [CrossRef]
33. Munirasu, S.; Banat, F.; Durrani, A.A.; Haija, M.A. Intrinsically superhydrophobic PVDF membrane by phase inversion for membrane distillation. *Desalination* **2017**, *417*, 77–86. [CrossRef]
34. Hou, D.; Fan, H.; Jiang, Q.; Wang, J.; Zhang, X. Preparation and characterization of PVDF/nonwoven fabric flat-sheet composite membranes for desalination through direct contact membrane distillation. *Sep. Purif. Technol.* **2014**, *135*, 211–222. [CrossRef]
35. Thomas, R.; Guillen-Burrieza, E.; Arafat, H.A. Pore structure control of PVDF membranes using a 2-stage coagulation bath phase inversion process for application in membrane distillation (MD). *J. Membr. Sci.* **2014**, *452*, 470–480. [CrossRef]
36. Baghbanzadeh, M.; Rana, D.; Matsuura, T.; Lan, C.Q. Effects of hydrophilic CuO nanoparticles on properties and performance of PVDF VMD membranes. *Desalination* **2015**, *369*, 75–84. [CrossRef]
37. Ahmad, A.; Ramli, W. Hydrophobic PVDF membrane via two-stage soft coagulation bath system for Membrane Gas Absorption of CO_2. *Sep. Purif. Technol.* **2013**, *103*, 230–240. [CrossRef]
38. Chang, H.-H.; Chang, L.-K.; Yang, C.-D.; Lin, D.-J.; Cheng, L.-P. Effect of polar rotation on the formation of porous poly (vinylidene fluoride) membranes by immersion precipitation in an alcohol bath. *J. Membr. Sci.* **2016**, *513*, 186–196. [CrossRef]
39. Kuo, C.-Y.; Lin, H.-N.; Tsai, H.-A.; Wang, D.-M.; Lai, J.-Y. Fabrication of a high hydrophobic PVDF membrane via nonsolvent induced phase separation. *Desalination* **2008**, *233*, 40–47. [CrossRef]
40. Park, Y.; Ju, J.; Woo, Y.; Choi, J.-S.; Lee, S. Fabrication and characterization of moderately hydrophobic membrane with enhanced permeability using a phase-inversion method in membrane distillation. *Desalination Water Treat.* **2020**, *183*, 173–181. [CrossRef]
41. Kim, Y.; Choi, Y.; Choi, J.; Lee, S. Powdered activated carbon (PAC)—vacuum-assisted air gap membrane distillation (V-AGMD) hybrid system to treat wastewater containing surfactants: Effect of operating conditions. *Environ. Eng. Res.* **2021**, *26*, 200377. [CrossRef]
42. Tijing, L.D.; Woo, Y.C.; Johir, M.A.H.; Choi, J.-S.; Shon, H.K. A novel dual-layer bicomponent electrospun nanofibrous membrane for desalination by direct contact membrane distillation. *Chem. Eng. J.* **2014**, *256*, 155–159. [CrossRef]
43. Choudhury, M.R.; Anwar, N.; Jassby, D.; Rahaman, M.S. Fouling and wetting in the membrane distillation driven wastewater reclamation process–A review. *Adv. Colloid Interface Sci.* **2019**, *269*, 370–399. [CrossRef] [PubMed]
44. Choi, Y.; Choi, J.; Shin, Y.; Cho, H.; Sohn, J.; Lee, S. A feasibility study on sewage discharge water treatment for water reuse by direct contact membrane distillation. *Membr. J.* **2016**, *26*, 70–75. [CrossRef]

45. Khayet, M.; Matsuura, T. Chapter 10—Direct Contact Membrane Distillation. In *Membrane Distillation*; Khayet, M., Matsuura, T., Eds.; Elsevier: Amsterdam, The Netherlands, 2011; pp. 249–293.
46. Rahimpour, M.R.; Esmaeilbeig, M.A. Chapter 6—Membrane Wetting in Membrane Distillation. In *Current Trends and Future Developments on (Bio-) Membranes*; Basile, A., Curcio, E., Inamuddin, Eds.; Elsevier: Melbourne, Australia, 2019; pp. 143–174.
47. Servi, A.T.; Kharraz, J.; Klee, D.; Notarangelo, K.; Eyob, B.; Guillen-Burrieza, E.; Liu, A.; Arafat, H.A.; Gleason, K.K. A systematic study of the impact of hydrophobicity on the wetting of MD membranes. *J. Membr. Sci.* **2016**, *520*, 850–859. [CrossRef]
48. Kim, B.-S.; Harriott, P. Critical entry pressure for liquids in hydrophobic membranes. *J. Colloid Interface Sci.* **1987**, *115*, 1–8. [CrossRef]
49. Pagliero, M.; Bottino, A.; Comite, A.; Costa, C. Novel hydrophobic PVDF membranes prepared by nonsolvent induced phase separation for membrane distillation. *J. Membr. Sci.* **2020**, *596*, 117575. [CrossRef]
50. Guillen, G.R.; Pan, Y.; Li, M.; Hoek, E.M. Preparation and characterization of membranes formed by nonsolvent induced phase separation: A review. *Ind. Eng. Chem. Res.* **2011**, *50*, 3798–3817. [CrossRef]